CrossMark

Correction to the Photometric Colors of Gaia Early Data Release 3

Zexi Niu[1,2] , Haibo Yuan[3] , and Jifeng Liu[1]
[1] National Astronomical Observatories, Chinese Academy of Sciences, 20A Datun Road, Chaoyang District, Beijing, People's Republic of China
[2] University of Chinese Academy of Sciences, No.19(A) Yuquan Road, Shijingshan District, Beijing 100049, People's Republic of China
[3] Department of Astronomy, Beijing Normal University, 19th Xinjiekouwai Street, Haidian District, Beijing, People's Republic of China; yuanhb@bnu.edu.cn
Received 2021 January 12; revised 2021 January 29; accepted 2021 January 29; published 2021 February 15

Abstract

In this work, we use the spectroscopy-based stellar color regression method with ∼0.7 million common stars between LAMOST DR7 and Gaia EDR3 to acquire color corrections in $G - G_{RP}$ and $G_{BP} - G_{RP}$. A sub-millimagnitude precision is achieved. Our results demonstrate that improvements in the calibration process of the EDR3 have removed the color term in $G_{BP} - G_{RP}$ and eliminated the discontinuity caused by the changes of instrument configurations to a great extent. However, modest systematic trends with G magnitude are still detected. The corresponding color correction terms as a function of G are provided for 9.5 mag $< G <$ 17.5 mag and compared with other determinations. We conclude that the corrections given in this work are particularly suited for cases where the color–color investigations are required, while for color–magnitude investigations other corrections may be better owing to systematics with reddening. Possible applications of our results are discussed.

Unified Astronomy Thesaurus concepts: Stellar photometry (1620); Astronomy data analysis (1858); Fundamental parameters of stars (555)

1. Introduction

Very recently, Gaia Collaboration published the Early Data Release 3 (EDR3; Gaia Collaboration et al. 2020) based on the first 34 months of its nominal mission (Gaia Collaboration et al. 2016), providing G-band photometry for 1.8 billion sources brighter than 21 and 1.5 billion sources with G_{BP} and G_{RP} photometry, with a uniform calibration at millimagnitude level. In the Gaia DR2 era, several works have detected the magnitude-dependent systematic errors up to 10 mmag or higher (Casagrande & VandenBerg 2018; Maíz Apellániz & Weiler 2018; Weiler 2018; Niu et al. 2021) and the discontinuities caused by the changes of instrument configurations (Evans et al. 2018; Niu et al. 2021). Among them, using about 0.5 million well-selected common stars between the LAMOST DR5 (Zhao et al. 2012; Luo et al. 2015) and Gaia DR2, Niu et al. (2021, hereafter Paper I) applied the stellar color regression (SCR) method (Yuan et al. 2015) to calibrate the $G - G_{RP}$ and $G_{BP} - G_{RP}$ colors. With an unprecedented precision of about 1 mmag, systematic trends with G magnitude are revealed in great detail for both colors, reflecting changes in instrument configurations. Color-dependent trends are also found for the $G_{BP} - G_{RP}$ for stars brighter than $G \sim 11.5$ mag.

From DR2 (Gaia Collaboration et al. 2018) to EDR3, a number of important improvements have been implemented to further reduce its photometric (random and systematic) errors, including the fitting of G fluxes, the processing of BP and RP spectra, and the calibration processes (Fabricius et al. 2020; Riello et al. 2020). The median uncertainties of G magnitudes are reduced by almost a factor of two, reaching 0.2 mmag at 10 mag $< G <$ 14 mag, 0.8 mmag at $G \sim 17$ mag, and 2.6 mmag at $G \sim 19$ mag. In order to take full advantage of its exquisite photometric quality, in this work we follow the same routine as in Paper I to validate and correct possible magnitude/color-dependent systematics in EDR3.

The paper is organized as follows. We briefly describe our data and method in Section 2, with differences from Paper I stressed. The results are presented and discussed in Section 3. We summarize in Section 4.

2. Data and Method

We use the same method and follow the same steps as in Paper I, which are briefly summarized below. Details of criteria used to select samples and the SCR method can be found in Paper I.

We combine the newest Gaia EDR3 with the LAMOST DR7 (Luo et al. 2015) and apply the same constraints as in Paper I, e.g., $E(B - V) < 0.05$ mag according to the Schlegel et al. (1998, hereafter SFD) dust reddening map, galactic latitude $|b| > 20°$, and vertical distance to the galactic disk $|Z| > 0.2$ kpc. In Figure 3 of Paper I, we clarified that the signal-to-noise ratio for the g band (S/N$_g$) of 20 is sufficient for this work because there are no systematic effects in the LAMOST stellar parameters with the S/N$_g$ until at very low S/N$_g$ of about 15. So we adopt a lower cut on S/N$_g$ of 20 to generate a larger sample. At S/N$_g$ > 20, the agreement of the LAMOST parameters with APOGEE is better than 120 K for T_{eff}, 0.15 dex for log g, and 0.1 dex for [Fe/H], as shown in Figure 3 of Paper I.

We finally select a sample containing 779,691 main-sequence (MS) stars and 71,952 red giant branch (RGB) stars, covering the 9.5 mag $< G <$ 17.5 mag range. Note that as proposed by the Gaia Collaboration et al. (2020) and Riello et al. (2020), the corrected G magnitudes for sources with six-parameter astrometric solutions are used in this paper.

Due to the different passbands between DR2 and EDR3, their reddening coefficients are slightly different. Following Y. Sun et al. (2021, in preparation), we have empirically determined the temperature- and reddening-dependent reddening coefficients for the EDR3 colors, as given by the Equations (1) and (2). Note that the reddening corrections in this work do not take into account the distance of sources and assume that all sources are beyond the source of reddening. All colors referred to hereafter
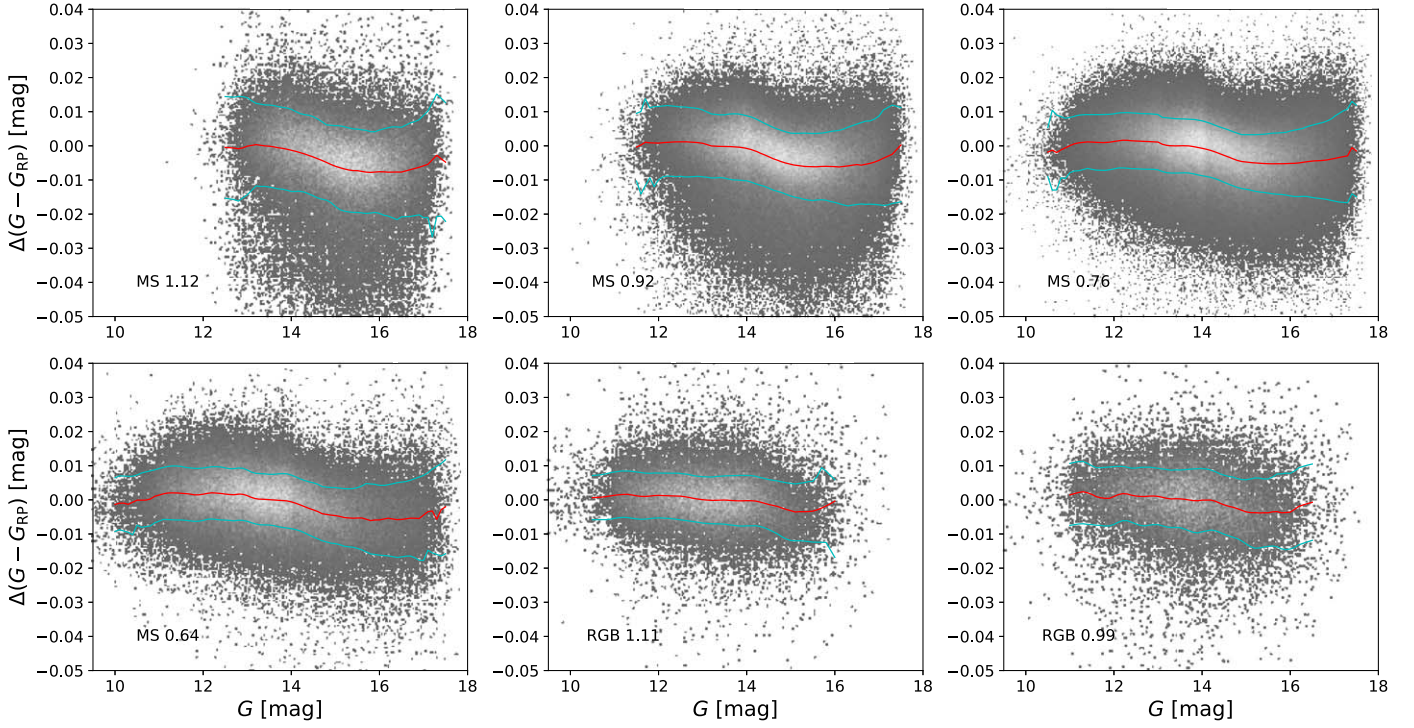
Figure 1. $G - G_{RP}$ residuals against G magnitude for six subsamples labeled by their evolution stages and median $(G_{BP} - G_{RP})_0$ colors. Red and cyan lines are the LOWESS (locally weighted scatterplot smoothing) of the median values and the standard deviations for the equally spaced G bins, respectively.

are dereddened using the SFD map and the empirical coefficients

$$R(G_{BP} - G) = 1.428 - 0.539 \times E(B - V)_{SFD} + 0.406$$
$$\times E(B - V)_{SFD}^2 - 1.976 \times 10^{-4} \times T_{eff} + 2.004 \times 10^{-5}$$
$$\times T_{eff} \times E(B - V)_{SFD} - 1.187 \times 10^{-8} \times T_{eff}^2$$

$$(1)$$

$$R(G_{BP} - G_{RP}) = 1.684 - 0.839 \times E(B - V)_{SFD} + 0.555$$
$$\times E(B - V)_{SFD}^2 - 1.390 \times 10^{-4} \times T_{eff} - 3.142 \times 10^{-6}$$
$$\times T_{eff} \times E(B - V)_{SFD} + 1.520 \times 10^{-8} \times T_{eff}^2.$$

$$(2)$$

As in Paper I, a control sample of 13.3 mag $< G <$ 13.7 mag is selected to define the empirical relations between the Gaia intrinsic colors and the LAMOST DR7 stellar parameters. Then, we divide the selected samples into six subsamples of different evolution stages and colors. MS stars are divided into four subsamples with the median $G_{BP} - G_{RP}$ colors of 1.12, 0.92, 0.76, and 0.64 mag, respectively. RGB stars are divided into two subsamples, with the median $G_{BP} - G_{RP}$ colors of 1.11 and 0.99 mag, respectively. Applying these relations to a given (sub)sample, the median values of the color residuals between the SCR-derived colors and the corresponding Gaia EDR3 ones as a function of G are obtained as the correction terms, as shown in Figures 1 and 2. A 3σ clipping is performed in the process. Specifically, corrections can be expressed as

$$C' = C + \Delta C, \qquad (3)$$

where C' is the corrected color, C is the Gaia EDR3 color, and ΔC is the color correction term.

3. Result and Discussion

Figure 3 plots color correction curves yielded by different subsamples. As already demonstrated in Paper I, (1) the correction

terms are independent of the stellar evolution stages, and (2) the inconsistency between the red and blue subsamples when $G > 14$ mag is due to the selection function of the LAMOST data and the spatially dependent systematics of the SFD reddening map. Therefore, we compute the recommended correction curves using the three blue MS subsamples (MS 0.92, MS 0.76, and MS 0.64). The results are overplotted with black lines in Figure 3 and listed in Table 1. The standard deviations of the difference between the recommended curve and the three blue MS subsamples for $G - G_{RP}$ and $G_{BP} - G_{RP}$ are 0.3 and 0.7 mmag, respectively. This suggests that the calibration curve of each subsample has a typical random error smaller than 1.0 mmag, and the random errors of the recommended curves are even smaller. In the top panel of Figure 3, the systematic trend of $G - G_{RP}$ is smaller than the one found for Gaia DR2, with a maximum range of less than 10 mmag in total. The feature coming from the observation modes changing at $G \sim 16$ mag is gone, and those at $G \sim 11$ and 13 mag are visible but at a level of about 1 mmag from the recommended curve. This confirms the big improvement in the G-band photometry. The bottom panel shows that the $G_{BP} - G_{RP}$ correction curves are no longer color dependent at the bright end, at least for F/G/K stars. However, the magnitude-dependent trend is still significant, as in DR2.

To test our color correction curves, we select an MS sample within a narrow [Fe/H] range of $-0.5 <$ Fe/H < -0.25 and compare their distributions in the color–color diagram before and after corrections using the recommended curves in Table 1. The results are shown in the left panels of Figure 4. Magnitude-dependent offsets in the color–color diagram are clearly seen from the top left panel. After corrections, there are no offsets, and the total width becomes narrower as expected. Furthermore, like Figure 32 in Fabricius et al. (2020) of EDR3 and Figure 31 in Arenou et al. (2018) of DR2, we plot a 2D histogram of the $G - G_{RP}$ residuals in the right panels of
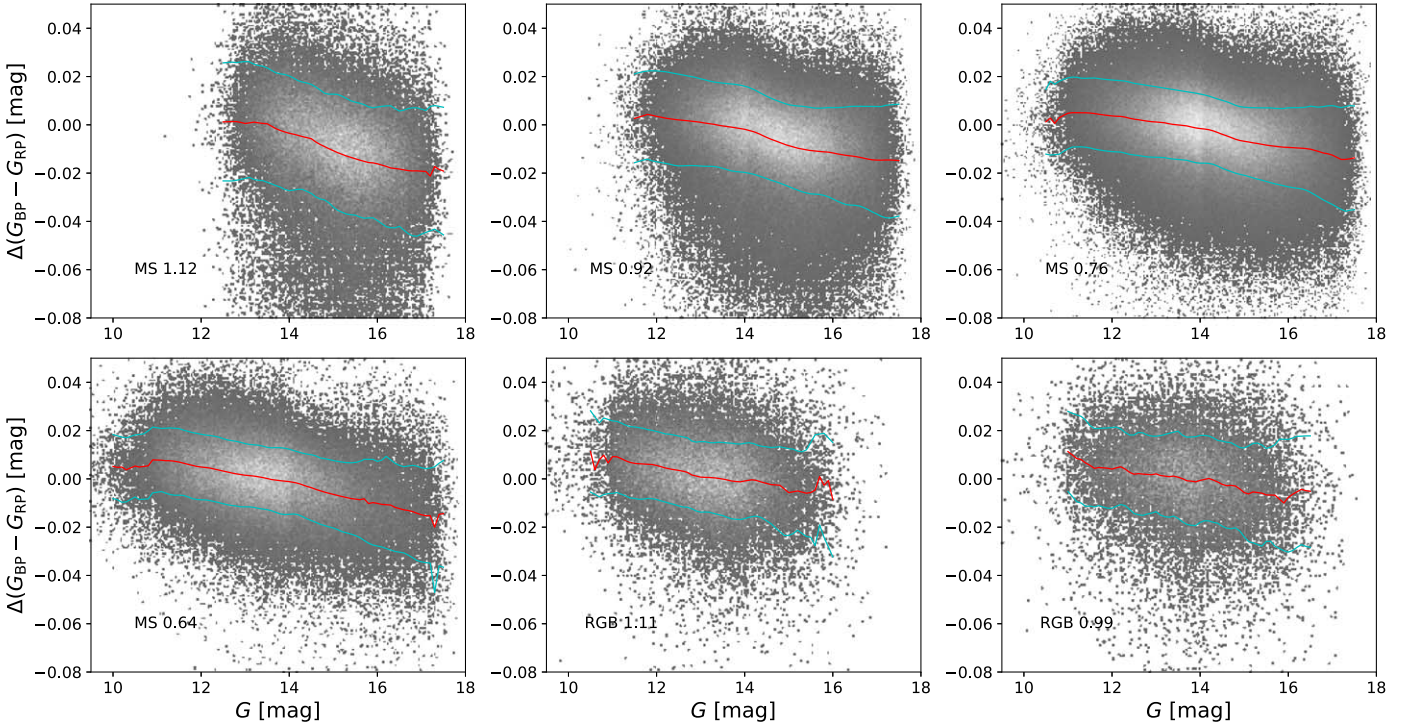
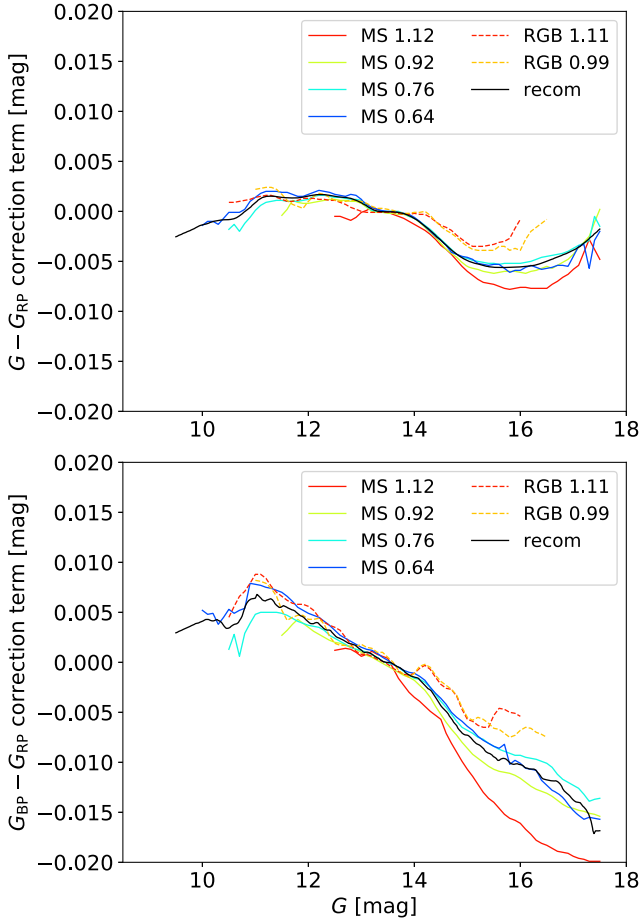**Figure 2.** Same as Figure 1, but for $G_{BP} - G_{RP}$ residuals.

Figure 3. Color correction curves yielded by different subsamples and the recommended ones for $G - G_{RP}$ (top) and $G_{BP} - G_{RP}$ (bottom).

Figure 4 with respect to the metallicity-dependent stellar color locus. The improved yet still subsistent trend with magnitude is clearly seen in the top panel, especially at the bright and faint ends. After corrections of this work, the trend becomes flat and centered at zero, demonstrating the power of our corrections in the color–color diagram.

There are also color corrections deduced from other approaches. For example, using 10,000 well-selected Landolt standard stars (Clem & Landolt 2013), Yang et al. (2021) have obtained magnitude and color corrections of the Gaia EDR3 by training the observed *UBVRI* magnitudes into the Gaia EDR3 magnitudes and colors. Their results (red lines in their Figure 4) are plotted with green lines in Figure 5. Results from synthetic colors of the CALSPEC (Bohlin 2014) spectra are also plotted with black circles. Only 61 stars with `phot_bp_rp_excess_factor` < 0.1 after Riello et al. (2020) correction and $G > 8$ mag are shown. Note that Yang et al. (2021) adopted a control sample of 17 mag $< G <$ 17.5 mag, and their correction curves were shifted to match the results of the CALSPEC spectra. In this work, we have adopted a different control sample of 13.2 mag $< G <$ 13.6 mag; therefore, a constant offset may well exist. To make a straightforward comparison, the recommended curves in this work, which are overplotted with red solid lines, are systematically shifted by a few millimagnitudes to match the Yang et al. (2021) corrections at 14 mag. Given the small number of black circles and their internal scatter (about 10 mmag for $G - G_{RP}$ and 15 mmag for $G_{BP} - G_{RP}$), results from both this work and Yang et al. (2021) are consistent with the black circles. However, discrepancies between this work and Yang et al. (2021) are up to about ± 5 mmag for $G - G_{RP}$ and ± 10 mmag for $G_{BP} - G_{RP}$ and are correlated with the G magnitude.

To investigate the origins and effects of the discrepancies between this work and Yang et al. (2021), their differences of the color corrections without shifting in $G_{BP} - G_{RP}$ are plotted against

4

Table 1
Color Correction Curves

G	recom		G	recom		G	recom		G	recom		G	recom		G	recom	
9.50	−2.54	2.95	10.85	0.17	6.00	12.20	1.68	3.84	13.55	−0.04	−0.02	14.90	−4.65	−7.07	16.25	−5.41	−10.68
9.53	−2.48	3.01	10.88	0.30	6.19	12.23	1.68	3.68	13.58	−0.04	−0.10	14.93	−4.74	−7.19	16.28	−5.38	−10.75
9.56	−2.39	3.10	10.91	0.43	6.30	12.26	1.69	3.55	13.61	−0.06	−0.21	14.96	−4.81	−7.26	16.31	−5.33	−10.90
9.59	−2.33	3.16	10.94	0.60	6.36	12.29	1.68	3.39	13.64	−0.07	−0.32	14.99	−4.90	−7.28	16.34	−5.28	−11.09
9.62	−2.26	3.24	10.97	0.74	6.38	12.32	1.66	3.29	13.67	−0.09	−0.41	15.02	−4.96	−7.34	16.37	−5.24	−11.28
9.65	−2.18	3.32	11.00	0.87	6.42	12.35	1.64	3.23	13.70	−0.11	−0.47	15.05	−5.01	−7.46	16.40	−5.17	−11.53
9.68	−2.12	3.38	11.03	1.00	6.79	12.38	1.62	3.23	13.73	−0.14	−0.54	15.08	−5.07	−7.64	16.43	−5.12	−11.66
9.71	−2.04	3.46	11.06	1.15	6.66	12.41	1.59	3.20	13.76	−0.18	−0.66	15.11	−5.12	−7.83	16.46	−5.07	−11.71
9.74	−1.98	3.53	11.09	1.25	6.50	12.44	1.56	3.03	13.79	−0.21	−0.78	15.14	−5.17	−7.97	16.49	−5.00	−11.75
9.77	−1.92	3.60	11.12	1.34	6.32	12.47	1.53	2.86	13.82	−0.26	−0.94	15.17	−5.22	−8.13	16.52	−4.94	−11.77
9.80	−1.84	3.68	11.15	1.41	6.20	12.50	1.50	2.71	13.85	−0.32	−1.09	15.20	−5.26	−8.21	16.55	−4.89	−11.80
9.83	−1.77	3.75	11.18	1.46	6.15	12.53	1.47	2.55	13.88	−0.38	−1.20	15.23	−5.30	−8.28	16.58	−4.82	−11.85
9.86	−1.69	3.83	11.21	1.50	6.21	12.56	1.45	2.46	13.91	−0.46	−1.31	15.26	−5.35	−8.41	16.61	−4.77	−11.87
9.89	−1.60	3.90	11.24	1.51	6.27	12.59	1.44	2.41	13.94	−0.53	−1.38	15.29	−5.39	−8.55	16.64	−4.69	−11.85
9.92	−1.52	3.93	11.27	1.52	6.33	12.62	1.42	2.33	13.97	−0.60	−1.43	15.32	−5.43	−8.73	16.67	−4.63	−11.85
9.95	−1.43	4.00	11.30	1.52	6.33	12.65	1.40	2.25	14.00	−0.72	−1.48	15.35	−5.48	−8.92	16.70	−4.57	−11.92
9.98	−1.38	4.06	11.33	1.52	6.20	12.68	1.39	2.15	14.03	−0.81	−1.52	15.38	−5.50	−9.04	16.73	−4.50	−12.05
10.01	−1.35	4.13	11.36	1.50	5.97	12.71	1.38	2.06	14.06	−0.90	−1.56	15.41	−5.54	−9.10	16.76	−4.44	−12.24
10.04	−1.31	4.23	11.39	1.48	5.76	12.74	1.36	1.96	14.09	−1.02	−1.68	15.44	−5.56	−9.17	16.79	−4.38	−12.51
10.07	−1.26	4.28	11.42	1.47	5.61	12.77	1.33	1.89	14.12	−1.14	−1.86	15.47	−5.57	−9.30	16.82	−4.32	−12.79
10.10	−1.21	4.29	11.45	1.43	5.49	12.80	1.30	1.86	14.15	−1.24	−2.03	15.50	−5.59	−9.45	16.85	−4.26	−12.97
10.13	−1.15	4.25	11.48	1.41	5.50	12.83	1.25	1.81	14.18	−1.39	−2.22	15.53	−5.60	−9.55	16.88	−4.18	−13.11
10.16	−1.09	4.18	11.51	1.39	5.61	12.86	1.20	1.75	14.21	−1.51	−2.39	15.56	−5.61	−9.70	16.91	−4.12	−13.24
10.19	−1.04	4.15	11.54	1.38	5.65	12.89	1.14	1.69	14.24	−1.63	−2.54	15.59	−5.62	−9.79	16.94	−4.05	−13.40
10.22	−0.99	4.16	11.57	1.37	5.57	12.92	1.05	1.54	14.27	−1.79	−2.67	15.62	−5.63	−9.73	16.97	−3.95	−13.60
10.25	−0.96	4.23	11.60	1.36	5.49	12.95	0.98	1.41	14.30	−1.91	−2.77	15.65	−5.63	−9.63	17.00	−3.88	−13.77
10.28	−0.93	4.27	11.63	1.34	5.40	12.98	0.91	1.30	14.33	−2.06	−2.95	15.68	−5.62	−9.61	17.03	−3.80	−13.89
10.31	−0.89	4.17	11.66	1.34	5.33	13.01	0.83	1.17	14.36	−2.22	−3.18	15.71	−5.61	−9.63	17.06	−3.71	−13.97
10.34	−0.87	4.08	11.69	1.34	5.25	13.04	0.72	1.03	14.39	−2.35	−3.39	15.74	−5.61	−9.72	17.09	−3.62	−13.99
10.37	−0.86	3.92	11.72	1.34	5.21	13.07	0.64	0.99	14.42	−2.52	−3.71	15.77	−5.60	−9.86	17.12	−3.53	−14.03
10.40	−0.84	3.69	11.75	1.34	5.12	13.10	0.55	1.01	14.45	−2.65	−3.94	15.80	−5.59	−10.02	17.15	−3.39	−14.18
10.43	−0.84	3.50	11.78	1.34	4.97	13.13	0.45	0.99	14.48	−2.78	−4.14	15.83	−5.57	−10.13	17.18	−3.27	−14.39
10.46	−0.83	3.39	11.81	1.35	4.83	13.16	0.36	0.94	14.51	−2.95	−4.40	15.86	−5.56	−10.19	17.21	−3.15	−14.53
10.49	−0.83	3.41	11.84	1.37	4.70	13.19	0.25	0.83	14.54	−3.08	−4.58	15.89	−5.55	−10.19	17.24	−2.99	−14.73
10.52	−0.81	3.48	11.87	1.39	4.62	13.22	0.18	0.73	14.57	−3.23	−4.74	15.92	−5.55	−10.15	17.27	−2.86	−15.01
10.55	−0.78	3.63	11.90	1.42	4.54	13.25	0.12	0.63	14.60	−3.39	−4.91	15.95	−5.55	−10.15	17.30	−2.72	−15.37
10.58	−0.76	3.73	11.93	1.47	4.39	13.28	0.06	0.52	14.63	−3.52	−5.09	15.98	−5.55	−10.21	17.33	−2.57	−15.84
10.61	−0.71	3.80	11.96	1.50	4.23	13.31	0.02	0.44	14.66	−3.69	−5.36	16.01	−5.55	−10.25	17.36	−2.45	−16.56
10.64	−0.64	3.85	11.99	1.53	4.08	13.34	−0.01	0.34	14.69	−3.82	−5.57	16.04	−5.54	−10.31	17.39	−2.28	−17.13
10.67	−0.56	3.94	12.02	1.56	3.95	13.37	−0.03	0.22	14.72	−3.94	−5.78	16.07	−5.54	−10.44	17.42	−2.15	−16.85
10.70	−0.43	4.17	12.05	1.59	3.87	13.40	−0.03	0.11	14.75	−4.10	−6.04	16.10	−5.52	−10.55	17.45	−2.03	−16.86
10.73	−0.33	4.41	12.08	1.61	3.86	13.43	−0.04	0.03	14.78	−4.21	−6.21	16.13	−5.50	−10.59	17.48	−1.86	−16.85
10.76	−0.21	4.74	12.11	1.62	3.90	13.46	−0.04	0.01	14.81	−4.33	−6.45	16.16	−5.48	−10.64	17.51	−1.73	−16.83
10.79	−0.06	5.32	12.14	1.64	3.96	13.49	−0.04	0.01	14.84	−4.45	−6.71	16.19	−5.47	−10.68			
10.82	0.05	5.71	12.17	1.66	3.97	13.52	−0.04	0.01	14.87	−4.54	−6.89	16.22	−5.45	−10.68			

Note. The first column is G magnitude. The second and third columns are, respectively, recommended $G - G_{RP}$ and $G_{BP} - G_{RP}$ calibration terms in units of mmag.

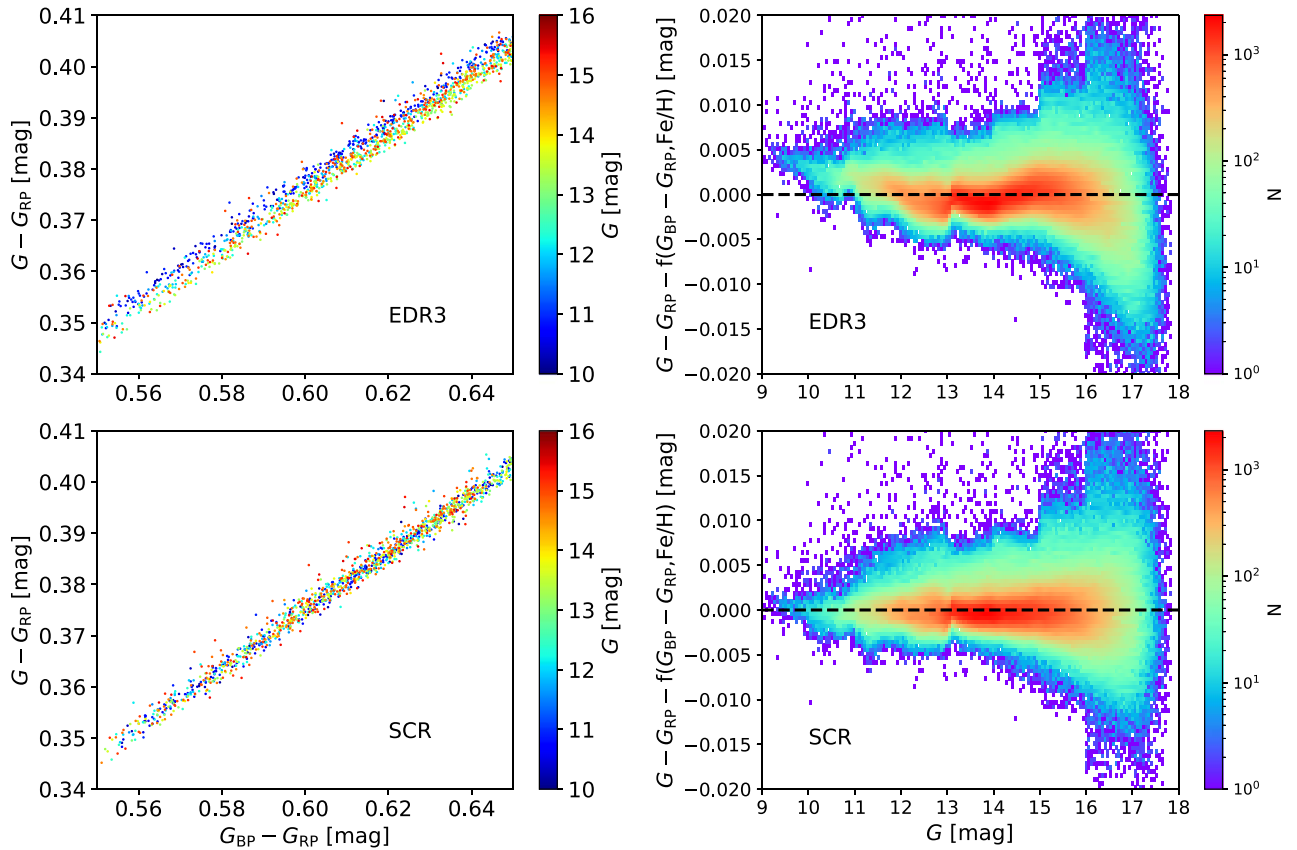**Figure 4.** From top to bottom: before and after color corrections. Left: color–color diagram of an MS sample within a narrow [Fe/H] range. Right: residuals from a global $G - G_{\rm RP} = f(G_{\rm BP} - G_{\rm RP}, {\rm [Fe/H]})$ relation.

those in $G - G_{\rm RP}$ in the bottom panel of Figure 5. A strong linear correlation is found. The slope is in good agreement with the median value of $\frac{R(G-G_{\rm RP})}{R(G_{\rm BP}-G_{\rm RP})}$. Considering that reddening corrections are not involved in Yang et al. (2021), the result suggests that the discrepancies are mainly caused by imperfect reddening corrections in this work. We use the 2D SFD reddening map. Despite the systematic errors that depend on spatial position and dust temperature (e.g., Peek & Graves 2010; Y. Sun et al. 2021, in preparation) in the SFD reddening map as discussed in Paper I, the map also tends to overestimate reddening for stars that are within the Galactic dust layer. Although in this work (and Paper I) we require stars of $|Z| > 0.2$ kpc, their reddening corrections may be overestimated to some extent around 0.01 mag in $E(B - V)$, depending on their distances/magnitudes. This is not surprising, as there is increasing evidence supporting the coexistence of a thin dust disk and a thick dust disk in the Galaxy (e.g., Guo et al. 2021; H.-B. Yuan et al. 2021, in preparation; R.-Y. Zhang et al. 2021, in preparation). The scale height of the thick dust disk is about 200–400 pc in the solar neighborhood. Dust clouds in the Galactic halo (H.-B. Yuan et al. 2021, in preparation) and halos of other galaxies (e.g., M31 and M33; Zhang & Yuan 2020) are also detected. We redo the procedure with an excessive sample of $|Z| > 1$ kpc and a control sample of 15.3 mag $< G < 15.5$ mag. Its results are plotted with red dashed lines, which match the green lines much better, consistent with the above scenario. This suggests that our correction curves of individual colors are subject to systematic errors from reddening correction using the SFD map. We further test other 2D reddening maps of Lenz et al. (2017), Peek & Graves (2010), and Planck Collaboration et al. (2014) and find no big differences with the SFD map.

Fortunately, even though both correction curves of the two Gaia colors suffer systematic errors in reddening correction, their systematic errors are largely canceled in the color–color diagram, as the reddening vector is almost parallel to the stellar locus in the color–color diagram. We estimate the standard deviation of the differences between the purple points and their corresponding gray line, which is 0.3 mmag and contributed by the random errors of corrections from Yang et al. (2021) and this work. Given that the typical errors of color correction curves of Yang et al. (2021) are about 0.2–0.4 mmag, the small standard deviation of 0.3 mmag suggests that the typical uncertainties in this work are much smaller than 0.3 mmag. Moreover, with 0.7 million stars, our sample enables a much higher resolution in G magnitude, yielding improved corrections in the color–color diagram compared to Yang et al. (2021, see their Figure 5).

It is worth clarifying that our color corrections in this work and in Paper I are precise to sub-millimagnitude only in the cases where a color–color diagram is used. In other cases, for example, where a color–magnitude diagram is used, the corrections from Yang et al. (2021) are preferred. Another thing that should be mentioned is that we compute the curves within approximately 9.5 mag $< G <$ 17.5 mag and $0.6 < G_{\rm BP} - G_{\rm RP} < 1.3$, so for stars outside the above ranges, e.g., very blue stars brighter than $G \sim 13$ (Riello et al. 2020), the curves should be used with caution. Nevertheless, this corrected color–color diagram could be helpful in a number of studies, for example, determining reliable photometric metallicities for an enormous and magnitude-limited sample of stars from Gaia (S. Xu et al. 2021, in preparation) and estimating binary fractions of a volume-limited sample of stars (Z.-X. Niu et al. 2021, in preparation).
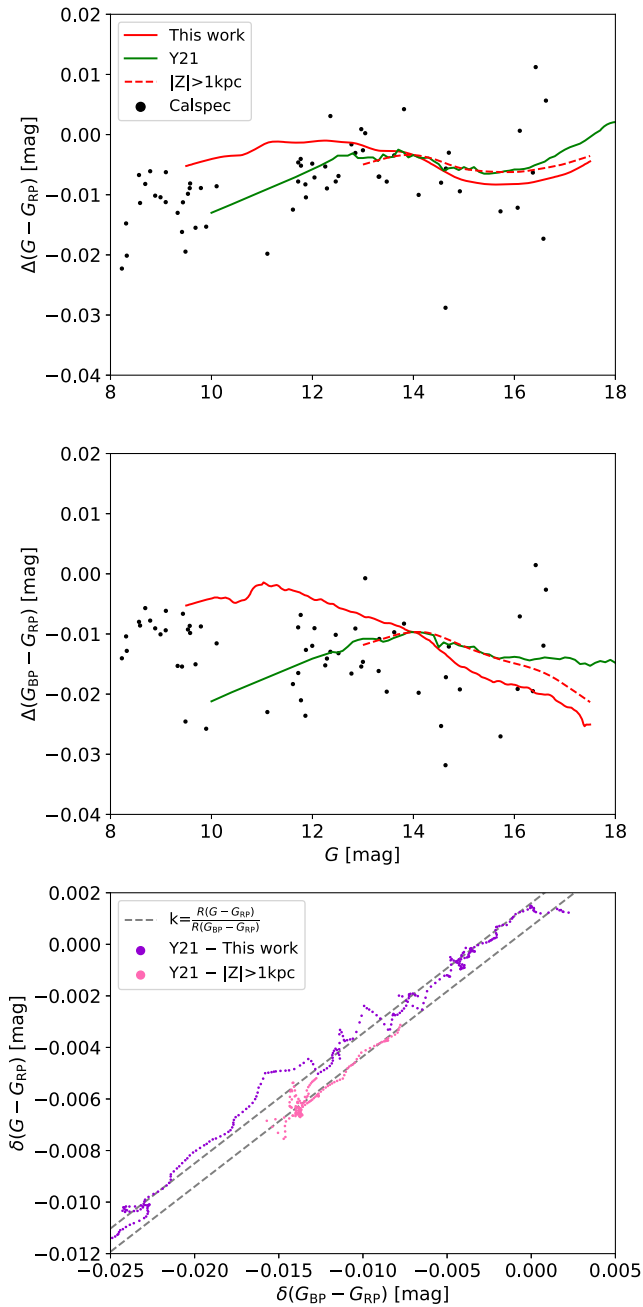
Figure 5. Top and middle: comparisons of different color correction curves. Red solid line: $|Z| > 0.2$ kpc using the SCR method. Red dashed line: $|Z| > 1$ kpc using the SCR method. Black circles: from the CALSPEC spectra. Green line: from Yang et al. (2021). Both red solid and dashed lines are systematically shifted by a few millimagnitudes to match the green lines at 14 mag for comparison. Bottom: differences of the color correction terms in $G_{BP} - G_{RP}$ vs. those in $G - G_{RP}$. The two dashed lines have the same slope, determined by the median value of $\frac{R(G - G_{RP})}{R(G_{BP} - G_{RP})}$.

4. Summary

Following Paper I, by combining $\sim$0.7 million high-quality common stars in LAMOST DR7 with the SCR method, we obtain $G - G_{RP}$ and $G_{BP} - G_{RP}$ color corrections as a function of G magnitude for 9.5 mag $< G <$ 17.5 mag to sub-millimagnitude precision for Gaia EDR3. Our results confirm the improvements in the calibration process of the EDR3. The color term of the $G_{BP} - G_{RP}$ for bright stars is removed. The

discontinuity caused by the changes of instrument configurations is significantly reduced. Yet modest systematic trends with G magnitude are detected.

By comparing with the work of Yang et al. (2021), we find that our color corrections of individual colors are subject to systematic errors in reddening correction with the SFD map. In the cases of color–color diagram, our corrections still achieve an unprecedented sub-millimagnitude precision. Our work could be beneficial to studies where a high-precision color–color diagram is required, including estimates of Gaia photometric metallicities and discrimination between binaries and single stars.

ORCID iDs

Zexi Niu ● https://orcid.org/0000-0002-3651-0681
Haibo Yuan ● https://orcid.org/0000-0003-2471-2363

References

Arenou, F., Luri, X., Babusiaux, C., et al. 2018, A&A, 616, A17
Bohlin, R. C. 2014, AJ, 147, 127
Casagrande, L., & VandenBerg, D. A. 2018, MNRAS Letters, 479, L102
Clem, J. L., & Landolt, A. U. 2013, AJ, 146, 88
Evans, D. W., Riello, M., De Angeli, F., et al. 2018, A&A, 616, A4
Fabricius, C., Luri, X., Arenou, F., et al. 2020, arXiv:2012.06242
Gaia Collaboration, Brown, A. G. A., Vallenari, A., et al. 2018, A&A, 616, A1
Gaia Collaboration, Brown, A. G. A., Vallenari, A., et al. 2020, arXiv:2012.01533
Gaia Collaboration, Prusti, T., de Bruijne, J. H. J., et al. 2016, A&A, 595, A1
Guo, H. L., Chen, B. Q., Yuan, H. B., et al. 2021, ApJ, 906, 47
Lenz, D., Hensley, B. S., & Doré, O. 2017, ApJ, 846, 38
Luo, A. L., Zhao, Y.-H., Zhao, G., et al. 2015, RAA, 15, 1095
Maíz Apellániz, J., & Weiler, M. 2018, A&A, 619, A180
Niu, Z., Yuan, H., & Liu, J. 2021, ApJ, in press (arXiv:2101.04290)
Peek, J. E. G., & Graves, G. J. 2010, ApJ, 719, 415
Planck Collaboration, Abergel, A., Ade, P. A. R., et al. 2014, A&A, 571, A11
Riello, M., De Angeli, F., Evans, D. W., et al. 2020, arXiv:2012.01916
Schlegel, D. J., Finkbeiner, D. P., & Davis, M. 1998, ApJ, 500, 525
Weiler, M. 2018, A&A, 617, A138
Yang, L., Yuan, H., Zhang, R., et al. 2021, ApJL, in press (arXiv:2101.00750)
Yuan, H., Liu, X., Xiang, M., et al. 2015, ApJ, 799, 133
Zhang, R., & Yuan, H. 2020, ApJ, 895, 20
Zhao, G., Zhao, Y.-H., Chu, Y.-Q., Jing, Y.-P., & Deng, L.-C. 2012, RAA, 12, 723